Spectroscopic Signature and Structure of Active Centers in Ziegler-Natta Polymerization Catalysts revealed by Electron Paramagnetic Resonance

A. Ashuiev[1‡], M. Humbert[2‡], S. Norsic[2], J. Blahut[3], D. Gajan[3], K. Searles[1], D. Klose[1], A. Lesage[3], G. Pintacuda[3], J. Raynaud[2*], V. Monteil[2*], C. Copéret[1*], G. Jeschke[1*]

[1]Department of Chemistry and Applied Biosciences, ETH Zurich, Wolfgang-Pauli-Strasse 1-5, 8093 Zurich, Switzerland.

[2]Université de Lyon, Univ. Lyon 1, CPE Lyon, CNRS, Chimie Catalyse Polymères et Procédés (C2P2), LCPP team, 43 Bd du 11 novembre 1918, 69616 Villeurbanne, France.

[3]Univ Lyon, ENS Lyon, Université Lyon 1, CNRS, High-Field NMR Center of Lyon, FRE 2034, F-69100 VILLEURBANNE, France.

*Email: jean.raynaud@univ-lyon1.fr (J. R.); vincent.monteil@univ-lyon1.fr (V. M.); ccoperet@inorg.chem.ethz.ch (C. C.); gunnar.jeschke@phys.chem.ethz.ch (G. J.)

‡A. Ashuiev and M. Humbert declare equal contribution.

Despite decades of extensive studies, the atomic-scale structure of active sites in heterogeneous Ziegler-Natta (ZN) catalysts remains elusive and a matter of debate. Here, the structure of polymerization ZN catalysts is elucidated from magnetic resonance experiments carried out on samples reacted with increasing amounts of BCl_3 so as to enhance the concentration of active sites and observe clear spectroscopic signatures. Notably, we show that EPR and NMR spectroscopy of the activated ZN catalysts enables to observe paramagnetic species whose amount increases in conjunction with the catalytic activity. The joint application of 2D HYSCORE experiments and DFT calculations reveals the presence of bimetallic alkyl-Ti(III),Al complexes that are assigned to the catalytic centers of $MgCl_2$-supported Ziegler-Natta catalysts.

EPR spectroscopy and activation with BCl_3 enable unraveling the active-center structure of Ziegler-Natta catalysts.

Nowadays, polymers and particularly plastics are the most common products of chemical industry, comprising nearly 80% of the worldwide industry output (*1*). Two important polymers, which are widely used for e.g. packaging and construction materials in modern times, are polyethylene and polypropylene; they together sum up to more than half of the total plastics production (*2*). Such mass production of polyethylene and polypropylene became possible only after discovery of transition metal-based catalysts in the second half of the 20th century, such as Ziegler-Natta catalysts (*3, 4*). With their ability to promote the synthesis of high-density linear polyethylene and stereoregular polypropylene under relatively mild conditions, the Ziegler-Natta catalysts are responsible nowadays for nearly 50% of worldwide production of polyethylene and around 95% of overall polypropylene production (*5*). The boom of their commercial usage arose with the development of heterogeneous $MgCl_2$-supported Ziegler-Natta catalysts ($TiCl_4/MgCl_2$ activated with Et_3Al) in the 1960s, which appeared to be nearly 100 times more active than the ones originally proposed by Ziegler and Natta (*5, 6*). Due to the enormous productivity of such catalysts

and their unprecedented ability to tune the properties of produced plastics in a controlled way, the supported Ziegler-Natta catalysts became a workhorse of modern polyolefin industry (*6*).

Knowledge of the structure of the corresponding active center(s) represents a crucial step for enabling further improvement of the Ziegler-Natta catalytic process. However, despite decades of extensive studies, the atomic-scale description of the catalyst active centers/sites (without or with coordinated monomer) remained so far elusive. Ziegler-Natta catalysts are typically prepared by impregnating a $MgCl_2$ support with $TiCl_4$ that needs to be first treated either mechanically (grinding/ball milling) or chemically with Lewis bases of different types, often oxygen-based such as diethers, alcohols, or THF (*6, 7*). The catalytic Ziegler-Natta polymerization then requires the activation of the obtained precatalyst with an alkylaluminium reagent acting as a co-catalyst, e.g. Et_3Al. According to the proposition of Cossee and Arlman (*8*), the active site shall include a metal-carbon bond in order to perform ethylene insertion, which points towards Ti alkyl species as the active centers; alkylation of $TiCl_4$ most likely occurs upon addition of aluminum alkyls (Fig. 1).

Based on the activity of homogeneous and supported group IV transition-metal metallocenes towards ethylene polymerization (*9 - 12*), for which cationic M(IV) alkyl species were found to be the active sites (*13*), Ti(IV) cationic alkyls (**A**, Fig. 1a) have been proposed as possible active centers of $MgCl_2$-supported Ziegler-Natta catalysts (*14*). On the other hand, the addition of aluminum alkyls leads to a reduction of a large amount of Ti(IV) (*15*). Based on the estimated correlation of polymerization activity with the general amount of Ti^{3+} species (*16*), Ti(III) alkyls (**B**, Fig. 1a) have been proposed to be the active species (*17*). This proposition is further supported by a recent finding that well-defined Ti(III) neutral alkyls are efficient ethylene polymerization catalysts, where the presence of an unpaired electron favors C_2H_4 polymerization (*18*), and by the activity of silica-supported Ti(III) hydrides towards ethylene polymerization (*19, 20*). In fact, Giulio Natta himself proposed that the Ziegler-Natta catalysts could be bimetallic Ti(III)—Al complexes containing organometallic bonds (*21*) that could be interpreted as Ti(III)-(μ_2-Cl)-(μ_2-R)-AlR_2 type (**C**, Fig. 1a). This structure is also the cornerstone of the Rodriguez-Van Looy mechanism (*22*), which extends upon Cossee & Arlman's and proposes a bimetallic species to explain the stereospecificity of ZN-catalyzed propylene polymerization (*22*). So far, however, there has been no direct evidence for any of these proposed structures.

The difficulty of spectroscopic characterization of the active species of heterogeneous Ziegler-Natta catalysts is mostly related to the small amounts of those sites compared to the overall Ti amount. This problem may be addressed by investigating catalysts treated with strong Lewis acids, e.g. BCl_3 (Fig. 1b), which has been shown to significantly enhance the catalytic activity and therefore the number of active sites (*23, 24*), thereby opening new opportunities to capture spectroscopic signatures. Here, we report the structural characterization by EPR and NMR spectroscopies of these highly active Ziegler-Natta catalysts for ethylene polymerization treated with different amounts of BCl_3. Figure 1a shows schematically the protocol used to prepare the ZN samples used in this study.

Spectroscopic identification of the active species of Ziegler-Natta heterogeneous catalysts

As previously observed (*24*), the addition of BCl_3 continuously increases the activity of the Ziegler-Natta catalyst from 9 $kg_{PE}\cdot(g_{cat}\cdot h)^{-1}$ up to the maximal value of 38 $kg_{PE}\cdot(g_{cat}\cdot h)^{-1}$ (Fig. 2a and Table S1). At the same time, the average molar masses M_n and M_w as well as the corresponding dispersity $Đ$ of produced polyethylene remain essentially the same upon BCl_3 addition. This is strong evidence that the structure of the active centers of the Ziegler-Natta catalysts is not changed

and that the active-site concentration increases with addition of BCl_3, as discussed in a previous investigation based on a combination of kinetics and polymerization results (*24*). The activation by Et_3Al of samples prepared with different BCl_3 loading (Fig. 1b) was studied by NMR and pulse EPR spectroscopies (see SM Materials and Methods). A low [Al]/[Ti] ratio (~10), ca. one order of magnitude lower than typical ratios employed in ZN-catalyzed polymerizations – 100 < [Al]/[Ti] < 400 (*24*), – was used for these experiments for practicality. Higher ratios are used for conventional polymerization runs to scavenge impurities from the reaction medium (present in monomer, solvents…) and to maintain high activities throughout the polymerization processes. To ensure that the observed spectroscopic signatures actually relate to active centers, which become active sites in the presence of ethylene, we verified that all alkylated materials prepared under the conditions for the NMR and EPR experiments also displayed the expected polymerization performances (see SM *Validation of Spectroscopic Methodology* for details, and Table S2).

We first investigated the samples via solid-state NMR. While the ^{11}B solid-state NMR spectrum of precatalysts (before Et_3Al addition) shows that all B-containing species are boron alkoxides, resulting from the reaction of BCl_3 with either THF or chlorobutanoxy ligands (Fig. S1) (*7*), a sharp signal associated with physisorbed triethylboron formation (BEt_3) is observed after activation with Et_3Al (Fig. S2). The addition of Et_3Al also leads to the appearance of paramagnetic signals at ca. –60 ppm in the ^1H solid-state NMR spectra (*25*) of Ziegler-Natta catalysts prepared with or without BCl_3 addition, that are likely related to the presence of Ti^{III} species in their vicinity (Fig. S3). These paramagnetic signals are noticeably more pronounced in the spectra of the BCl_3-treated samples (Fig. S3).

Consequently, we tried to identify these paramagnetic species by EPR spectroscopy at 10 K and 9.5 GHz on samples with different BCl_3 loading, i.e. B/Ti = 0, 2.60 and 4.10 (Fig. 2b). These spectra reveal two paramagnetic species, characterized by a broad line around 340-390 mT and a narrower line at 320-340 mT that corresponds to an axially symmetric species. A species with a signal very similar to the 340-390 mT band has been observed before and has been assigned to Ti(III) surface species on $MgCl_2$(110) (*26*). Only the 320-340 mT band grows with increasing amount of added BCl_3, but is already present as a weak signal without addition of BCl_3 (see Fig. 2c and Fig. S4 – S6). Each of the three CW EPR spectra, shown in Fig. 2b, was fitted by a superposition of four individual spectra, revealing nearly the same *g* tensor parameters for all samples (Table S3). Three mean sets of principal *g* values contributing to the 340-390 mT band are g_1 = [1.8167 1.8657 1.9156], g_2 = [1.8910 1.9402 1.9621], g_3 = [1.9642 1.9716 1.9902]. They are consistent with previously estimated *g* tensor parameters for the three different conformations of $TiCl_3$ on the different $MgCl_2$ surfaces (*26*).

We then focused on establishing the nature of the species with the nearly axially symmetric *g* tensor g_4 = [2.0023 2.0053 2.1289]. Being larger than or similar to the free electron *g* value (g_e), these principal *g* values are highly unusual for a Ti(III) species. On the other hand, the large *g* anisotropy makes assignment to an organic radical very unlikely. The *g* tensor with unexpectedly large principal values is reminiscent of a previous observation for the $3d^1$ 3,10,17,24-tetrasulphonatophthalocyanin (tspc) complex of V(IV)O, in particular, with its $g_{\|} > g_e$ (*27*), which indicates that the $g > g_e$ values for d^1 species are indeed possible (see also SM *g tensor calculations*). This, together with the large anisotropy, led us to attribute the observed species to a Ti(III) complex with a distinct electronic structure rather than to an organic radical. A similar species can be recognized as a weak contribution to Q-band EPR spectra that were obtained in previous work on catalysts that were not activated by BCl_3 (*26*), but this species has not been

further discussed. We found that it was strongly suppressed in 35.7 GHz pulse EPR echo-detected spectra (Fig. S4), whereas it was readily observed in 9.5 GHz echo-detected EPR spectra (Fig. 2c). Since strong suppression of the $TiCl_3$ echo signals at 9.5 GHz is beneficial for characterizing the $g > 2$ species, further pulse EPR studies of the samples of $MgCl_2$-supported Ziegler-Natta catalysts with different BCl_3 loading were performed at this frequency (Fig. 2c). Like the CW EPR of this species, the echo-detected EPR signal, shown in Fig. 2c, continuously grew in intensity with increasing BCl_3 loading and thus paralleled the increasing catalyst activity (Fig. 2a). Therefore, we identify this $g > 2$ species (Fig. 2 b & c, marked with arrows) as the active centers of $MgCl_2$-supported Ziegler-Natta catalysts.

Evaluation of structure of the active centers

We further characterized this species by the 2D hyperfine spectroscopy technique HYSCORE (*28*). For these studies, we selected the sample with the highest activity of 38 $kg_{PE}\cdot(g_{cat}\cdot h)^{-1}$ (B/Ti = 3 and Table S1) because of the presence of the highest concentration of active centers. The HYSCORE spectrum was measured at the maximum of the 9.5 GHz field-swept echo-detected EPR spectrum (Fig. 3a, marked with arrow).

HYSCORE spectroscopy (Fig. 3b) reveals the presence of ^{1}H and ^{27}Al nuclei, coupled to the paramagnetic center by magnetic hyperfine interaction. The experimental HYSCORE pattern was simulated by adjusting hyperfine and quadrupole coupling parameters (Fig. 3b, red). The estimated ^{1}H isotropic hyperfine coupling of $a_{iso}(^{1}H) = -7.5 \pm 0.5$ MHz is, in fact, typical for the protons of alkyl ligands in Ti(III) alkyl complexes (*18, 20*). Within a point-dipole approximation we find a relatively large average Ti···H distance of $r_{Ti\text{-}H} = 3.16 \pm 0.24$ Å, which suggests that only relatively weak α- or β-H agostic interactions are observed within the alkyl ligand(s) (*18, 20*). At the same time, the moderate ^{27}Al isotropic hyperfine coupling $a_{iso}(^{27}Al) = 1.5 \pm 0.2$ MHz indicates that the Al atom is in a proximity to the paramagnetic center, most likely being connected to it through one bridging atom (see SM *Evaluation of the structure of the active species*). Strong ^{27}Al quadrupole coupling $Q(^{27}Al) = -42 \pm 1$ MHz indicates low symmetry of the Al coordination geometry. No ^{11}B hyperfine couplings were observed in the HYSCORE spectra. This is consistent with the absence of any modifications of the active center upon BCl_3 addition that can be inferred from the similar features of the produced polyethylenes as previously mentioned (*24*), from the removal of B in the form of BEt_3 and from the unchanged g tensor principal values. The EPR data also agrees with the NMR data discussed above, namely the observation of ^{1}H paramagnetic NMR resonances (Fig. S3). Very importantly, all these materials with characteristic EPR Ti(III)-alkyl signatures are active in polymerization by sole addition of ethylene monomer (see Table S2). These EPR spectroscopic signatures are thus assigned to active centers.

Based on these conclusions, we performed a search through possible DFT models, including Ti(III) alkyls, bridging alkyls and alkoxides with various ways of coordination of indicated organometallic ligands and aluminum alkyls (Fig. S8 – S11). Among all the tested models, we found only one (Fig. 3c & S11, a), that provides DFT-calculated ^{1}H hyperfine couplings for all H atoms of the Ti-C_2H_5 ligand that are in line with the experimental ^{1}H HYSCORE pattern (Figs. 3d & S11, b – f), together with a reasonable fit of the DFT-computed ^{27}Al couplings to the ones observed experimentally (Table S4). As ^{1}H hyperfine couplings were previously found to act as fingerprints of the conformations of Ti(III) alkyl complexes (*18, 20*), we propose the structure, shown in Fig. 3c, as an active center of the Ziegler-Natta catalysts. Being essentially a Ti(III) metal-alkyl complex of a formula $[Ti(C_2H_5)Cl_2\text{-}(\mu\text{-}Cl)\text{-}Al(C_2H_5)_2]@MgCl_2$ (Fig. 3c), this structure is in fact in line with the original proposal of Giulio Natta regarding the active site of Ziegler-Natta

catalysts (*21*). With a calculated Ti-C-H angle of 98.64°, it displays an α-H agostic interaction. The Al atom is essentially *tris*-coordinated, except for a weak Al—H interaction (2.183 Å distance) with the β-H atom of Ti-C_2H_5 ligand. A similar structure of [Ti(C_2H_5)Cl_2-(μ-Cl)-(μ-C)-Al(C_2H_5)$_2$]@$MgCl_2$ (**C**, Fig. 1a & Fig. S9, b), which has the α-C atom of Ti-C_2H_5 ligand bridging between the Ti and Al atoms, is calculated to be slightly more stable by 4.0 kcal·mol^{-1} according to the DFT computation, but exhibits a strong mismatch between DFT-computed ^{1}H hyperfine couplings and the experimental HYSCORE spectrum (see Fig. S9, b). The former is likely more favorable experimentally due to specific local environments that are not included in our cluster model that was used to allow accurate EPR calculation but only takes into account the first coordination environment.

Having also a weak π character in the Ti-C bond, revealed by a deviation of the natural hybrid orbital (NHO) on carbon from the Ti–C axis ($\Theta_{NHO\text{-}C\text{-}Ti}$ = 9.0°), the evaluated structure of the active species (Fig. 3c & Fig. S11, a) is akin to β-diiminato Ti(III) alkyls, which were shown to participate in ethylene polymerization in the absence of co-activator (*18*). Such π character, being likely enhanced after ethylene coordination, favors ethylene insertion into the Ti-C bond, while electron transfer of unpaired electron density from SOMO to the π*(C_2H_4) orbital lowers the formation energy of π-ethylene complexes in d^1 metal alkyls (*18*). These factors make Ti(III) d^1 alkyl complexes efficient ethylene polymerization catalysts, which supports our proposition of [Ti(C_2H_5)Cl_2-(μ-Cl)-Al(C_2H_5)$_2$]@$MgCl_2$ species (Fig. 3c) to be the active centers of the Ziegler-Natta catalysts that become the active sites for polymerization in the presence of ethylene.

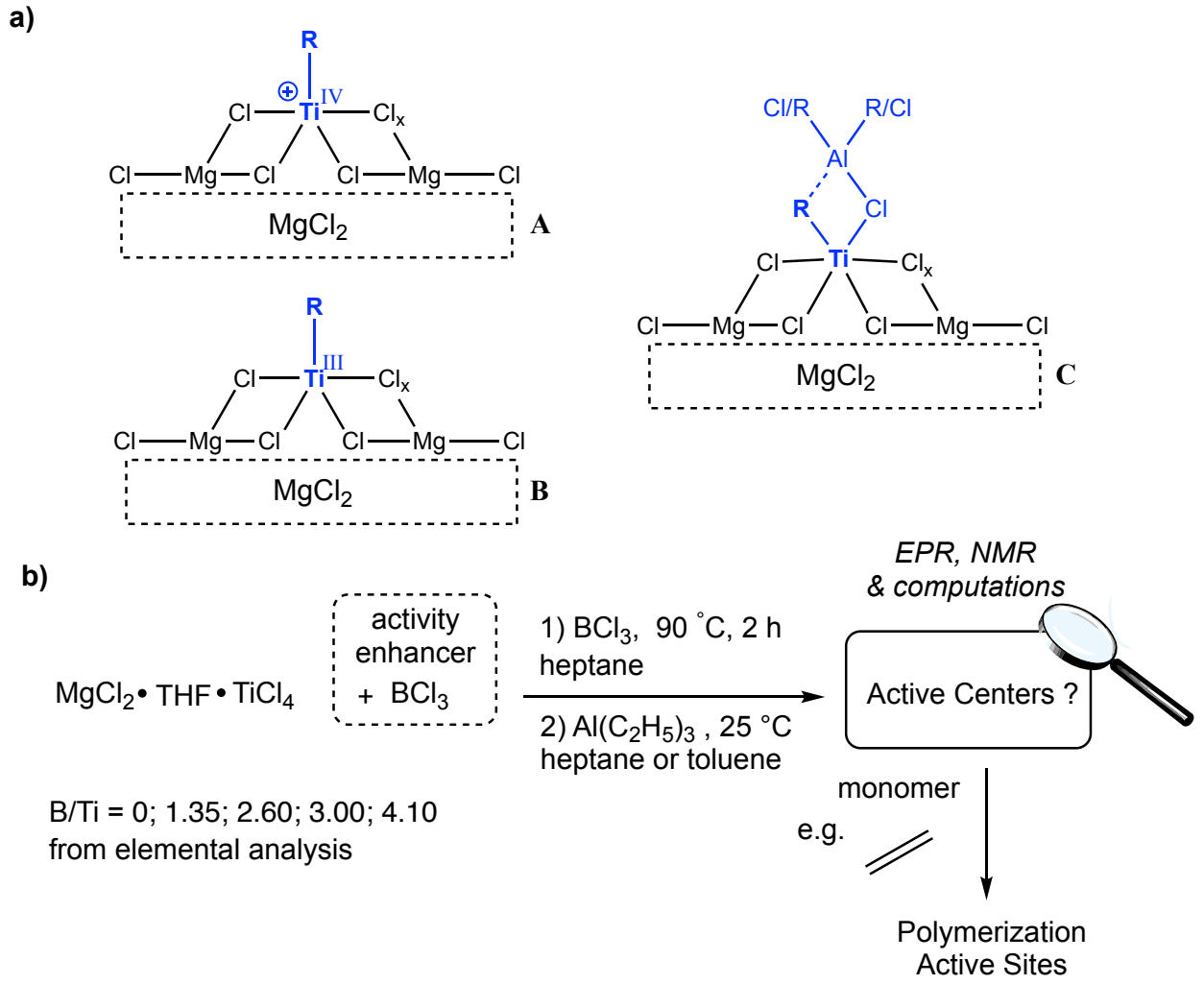

Figure 1. a) Possible active centers A-C of $MgCl_2$-supported Ziegler-Natta ethylene polymerization catalysts. b) Preparation of $MgCl_2$-supported Ziegler-Natta catalysts for ethylene polymerization as studied in the present work.

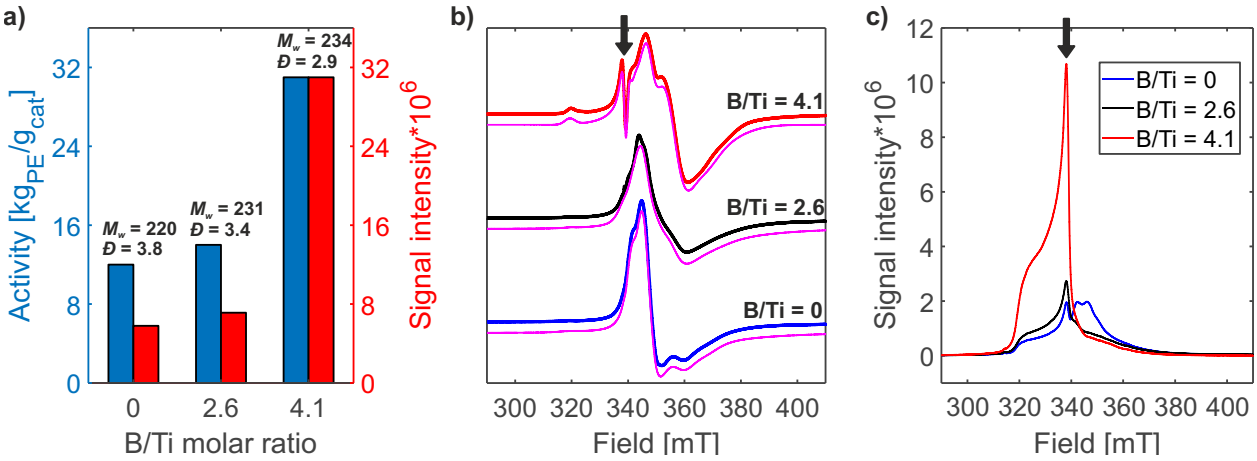

Figure 2. a) Change of activities towards ethylene polymerization (blue, right scale) and 9.5 GHz echo-detected EPR signal intensities (red, left scale) of Ziegler-Natta catalysts with a change of B/Ti ratio. For each catalyst, the average molar mass M_w [kg·mol^{-1}] and the dispersity $Đ = M_w/M_n$ of produced polyethylene are indicated. EPR signal intensities are measured at the field positions, marked with arrow in c), and normalized by the ratio of activity to intensity for the catalyst with B/Ti = 4.1. b) 9.5 GHz CW EPR spectra of Ziegler-Natta catalysts with B/Ti = 0 (blue), B/Ti = 2.6 (black) and B/Ti = 4.1 (red), together with the simulations (violet) of all the shown spectra (see text for parameters of the simulations). c) 9.5 GHz echo-detected EPR spectra of Ziegler-Natta catalysts with B/Ti = 0 (blue), B/Ti = 2.6 (black) and B/Ti = 4.1 (red). The signal that grows with increasing amount of added BCl_3 is indicated with arrows in b) and c).

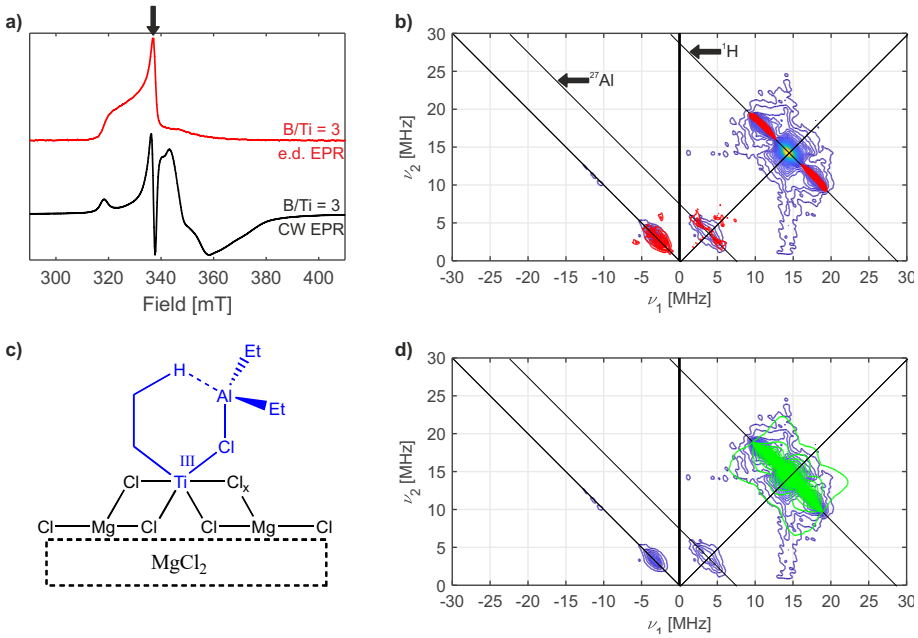

Figure 3. a) 9.5 GHz CW (black) and echo-detected (red) EPR spectra of Ziegler-Natta catalyst with B/Ti = 3. b) Experimental 9.5 GHz HYSCORE spectrum of Ziegler-Natta catalyst with B/Ti = 3, τ = [128 160 192] ns (blue to yellow), together with its simulation (red). c) Proposed structure of the active center of heterogeneous Ziegler-Natta catalysts (see also Fig. S11, a). d) Experimental HYSCORE spectrum of Ziegler-Natta catalyst with B/Ti = 3 (blue) and a simulation of experimental ^{1}H hyperfine couplings (green), based on DFT calculations on the proposed structure (see text & Fig. S11, b – f). The experimental HYSCORE spectrum (see Fig. S7) was measured at the magnetic field position indicated by an arrow in a).

Acknowledgments: We acknowledge Olivier Boyron, Manel Taam and Edgar Espinosa (Université de Lyon) for SEC analyses and Rene Tschaggelar (ETH Zürich) for the technical support in EPR experiments. **Funding:** A.A. is supported by a SNF—ANR grant (Mr. CAT 2-77275-15). M.H. is supported by a ANR-SNF grant (MRCAT ANR-15-CE29-0025) **Author contributions:** A.A. and M.H. declare equal contribution. A.A. performed EPR spectroscopy and DFT computations. M.H. carried out the synthesis of the catalysts and evaluated the polymerization activity studies. J. B and M. H. performed NMR measurements. S.N., D.G., K.S and D.K. supervised the project. C.C., G.J., J. R., V.M., A.L. and G.P. coordinated the project and provided guidance. All authors participated in writing the final manuscript. **Competing interests:** Authors declare no competing interests. **Data and materials availability:** All data is available in the main text or the supplementary materials.

References:

1. K. Singh, “Chemistry, Economics and Politics” in *Chemistry in Daily Life* (PHI Learning Pvt. Ltd., Delhi, 2012), pp. 132-134.

2. R. Geyer, J. R. Jambeck, K. L. Law, Production, use, and fate of all plastics ever made. *Sci. Adv.* **3** (7), e1700782 (2017).

3. K. Ziegler, E. Holzkamp, H. Breil, H. Martin, Das Mülheimer Normaldruck-Polyäthylen-Verfahren. *Angew. Chem.* **67**, 541-547 (1955).

4. G. Natta, Kinetic studies of α-olefin polymerization. *J. Polym. Sci.* **34** (127), 21-48 (1959).

5. N. Kashiwa, The discovery and progress of $MgCl_2$-supported $TiCl_4$ catalysts. *J. Polym. Sci. Part A* **42** (1), 1-8 (2004).

6. G. Cecchin, G. Morini, F. Piemontesi, "Ziegler-Natta catalysts" in *Kirk-Othmer Encyclopedia of Chemical Technology* (J. Wiley & Sons, New York, 2003), pp. 502-554.

7. E. Grau, A. Lesage, S. Norsic, C. Copéret, V. Monteil, P. Sautet, Tetrahydrofuran in $TiCl_4$/THF/$MgCl_2$: a Non-Innocent Ligand for Supported Ziegler–Natta Polymerization Catalysts. *ACS Catal.* **3** (1), 52-56 (2013).

8. E. J. Arlman, P. Cossee, Ziegler-Natta catalysis III. Stereospecific polymerization of propene with the catalyst system $TiCl_3$-$AlEt_3$. *J. Catal.* **3** (1), 99-104 (1964).

9. W. Kaminsky, Highly active metallocene catalysts for olefin polymerization. *J. Chem. Soc.* **9**, 1413-1418 (1998).

10. R. F. Jordan, W. E. Dasher, S. F. Echols, Reactive cationic dicyclopentadienyl zirconium(IV) complexes. *J. Am. Chem. Soc.* **108** (7), 1718-1719 (1986).

11. T. J. Marks, Surface-Bound Metal Hydrocarbyls. Organometallic Connections between Heterogeneous and Homogeneous Catalysis. *Acc. Chem. Res.* **25** (2), 57-65 (1992).

12. O. Olabisi, M. Atiqullah, W. Kaminsky, Group 4 Metallocenes: Supported and Unsupported. *J. Marcomol. Sci. Polymer Rev.* **37** (3), 519-554 (1997).

13. R. F. Jordan, Cationic Metal-Alkyl Olefin Polymerization Catalysts. *J. Chem. Educ.* **65** (4), 285-289 (1988).

14. Yu. V. Kissin, Active centers in Ziegler–Natta catalysts: Formation kinetics and structure. *J. Catal.* **292,** 188-200 (2012).

15. D. Fregonese, S. Mortara, S. Bresadola, Ziegler–Natta $MgCl_2$-supported catalysts: relationship between titanium oxidation states distribution and activity in olefin polymerization. *J. Mol. Catal. A: Chemical* **172** (1-2), 89-95 (2001).

16. E. I. Koshevoy, T. B. Mikenas, V. A. Zakharov, A. M. Volodin, R. M. Kenzhin, Formation of isolated titanium(III) ions in superactive titanium–magnesium catalysts with a low titanium content as active sites in ethylene polymerization. *Catal. Comm.* **48**, 38-40 (2014).

17. E. I. Koshevoy, T. B. Mikenas, V. A. Zakharov, A. A. Shubin, A. A. Barabanov, Electron Paramagnetic Resonance Study of the Interaction of Surface Titanium Species with AlR_3 Cocatalyst in Supported Ziegler–Natta Catalysts with a Low Titanium Content. *J. Phys. Chem. C* **120** (2), 1121-1129 (2016).

18. A. Ashuiev et al., https://chemrxiv.org/ndownloader/files/24060725

19. V. A. Zakharov, Yu. I. Yermakov, Supported Organometallic Catalysts for Olefin Polymerization. *Catal. Rev. Sci. Eng.* **19**, 67-103 (1979).

20. F. Allouche, D. Klose, C. P. Gordon, A. Ashuiev, M. Wörle, V. Kalendra, V. Mougel, C. Copéret, G. Jeschke, Low-Coordinated Ti(III) Alkyl-Molecular and Surface-Complexes: Detailed Structure from Advanced EPR Spectroscopy. *Angew. Chem. Int. Ed.* **57** (44), 14533-14537 (2018).

21. G. Natta, P. Pino, G. Mazzanti, U. Gianini, A crystallizable organometallic complex containing titanium and aluminium. *J. Am. Chem. Soc.* **79** (11), 2975-2976 (1957).

22. L. A. M. Rodriguez, H. M. Van Looy, Studies on Ziegler-Natta catalysts. Part V. Stereospecificity of the active center. *J. Polym. Sci.: Part A*-**1**, *4*, 1971-1992 (1966).

23. D. Ribour, V. Monteil, R. Spitz. Strong activation of $MgCl_2$-supported Ziegler-Natta catalysts by treatments with BCl_3: Evidence and application of the "cluster" model of active sites. *J. Polym. Sci. Part A* **47**, 5784-5791 (2009).

24. M. Humbert, S. Norsic, J. Raynaud, V. Monteil, Activity enhancement of $MgCl_2$-supported Ziegler-Natta catalysts by Lewis-Acid pre-treatment for ethylene polymerization. *Chinese J. Polym. Sci.* **37**, 1031-1038 (2019).

25. A. J. Pell, G. Pintacuda, C. P. Grey, Paramagnetic NMR in solution and the solid state. *Prog. Nucl. Mag. Res. Sp.* **111**, 1-271 (2019).

26. E. Morra, E. Giamello, S. Van Doorslaer, G. Antinucci, M. D'Amore, V. Busico, M. Chiesa, Probing the Coordinative Unsaturation and Local Environment of Ti^{3+} Sites in an Activated High-Yield Ziegler–Natta Catalyst. *Angew. Chem. Int. Ed.* **54** (16), 4857-4860 (2015).

27. A. Skorobogaty, R. Lancashire, T. D. Smith, J. R. Pilbrow, G. R. Sinclaire, Optical and Electron Spin Resonance Studies of Copper(II), Nickel(II) and Oxovanadium(IV) Complexes of Water-soluble Phthalocyanine and Porphyrazine Chelates Absorbed on Sephadex Resins, and the Effect of Added Dithionite. *J. Chem. Soc., Faraday Trans. 2* **79**, 1123-1141 (1983).

28. P. Höfer, A. Grupp, H. Nebenführ, M. Mehring, Hyperfine sublevel correlation (hyscore) spectroscopy: a 2D ESR investigation of the squaric acid radical. *Chem. Phys. Lett.* **132** (3), 279-282 (1986).